Simulating seawater intrusion in a complex coastal karst aquifer using an improved variable-density flow and solute transport–conduit flow process model

Zhongyuan Xu[1,2], Bill X. Hu[3,4], Zexuan Xu[5], Xiujie Wu[2]

[1] College of Earth, Ocean, and Environment, University of Delaware, Newark, DE 19716, USA [2] College of Environment & Civil Engineering, Chengdu University of Technology, Chengdu 610059, China [3] School of Water Resources and Environment, China University of Geosciences (Beijing), Beijing 100083, People's Republic of China [4] Institute of Groundwater and Earth Sciences, The Jinan University, Guangzhou 510632, Guangdong Province, People's Republic of China [5] Climate and Ecosystem Sciences Division, Lawrence Berkeley National Laboratory, Berkeley, CA 94720, USA

Zexuan Xu: xuzexuan@lbl.gov

Abstract

VDFST-CFP (variable-density flow and solute transport–conduit flow process) is a density-dependent discrete-continuum numerical model for simulating seawater intrusion in a dual-permeability coastal karst aquifer. A previous study (Xu and Hu 2017) simulates variable-density flow only in a single conduit, and studies the parameter sensitivities only in the horizontal case (2D domain as horizontal section) by the VDFST-CFP model. This paper focuses on the density-dependent vertical case (2D domain as vertical section) with two major improvements: 1) when implementing double-conduit networks in the domain, simulated intruded plumes in the porous medium are extended in the double-conduit scenario, compared to the single-conduit system; 2) by quantifying micro-textures on the conduit wall by the Goudar-Sonnad equation and considering macro-structures as local head loss. Sensitivity analysis shows that medium hydraulic conductivity, conduit diameter and effective porosity are important parameters for simulating seawater intrusion in the discrete-continuum system. On the other hand, rougher micro-structures and additional macro-structure components on the conduit wall would reduce the distance of seawater intrusion to the conduit system, but, rarely affect salinity distribution in the matrix. Compared to the equivalent mean roughness height, the new method (with more detailed description of structure) simulates seawater intrusion slightly landward in the conduit system. The macro-structure measured by local head loss is more reasonable but needs further study on conduit flow.

Keywords Karst . Numerical modeling . Seawater intrusion . VDFST-CFP

Introduction

Fresh groundwater in a coastal region can be easily contaminated by seawater intrusion, which is affected by sea level ris, regional precipitation deficit, and over-pumping. Seawater intrusion is related to several serious

environmental issues, including eco-alteration at the marine and estuarine areas, coastal groundwater contamination and soil salinization (Bear et al. 1999; Xu et al. 2018b). Coastal groundwater resources are particularly vulnerable to frequent seawater–freshwater exchanges in a karst aquifer, which consists of relative high-permeability conduits and low-permeability porous media. Submarine springs are usually observed and connected with the karst conduits in the aquifer. Depending on the hydraulic gradient, either freshwater discharge or seawater intrusion directions can be found in the submarine springs and connected karst conduits (Fleury et al. 2007). Groundwater flow in conduits is usually much faster than that in a porous medium, and may lead to long-distance seawater intrusion into a karst aquifer (Xu et al. 2016). Some studies indicate that intrusion through these submarine spring conduits fluctuates seasonally, associated with precipitation cycling (Arfib et al. 2006; Fleury et al. 2007; Davis and Verdi 2014; Xu et al. 2015b). However, the investigation of seawater intrusion through karst conduit systems is still a challenging issue due to the insufficient observational data, uncertain conduit geometry and the difficulties associated with underground conduit system exploration (Werner et al. 2013; Xu et al. 2016).

The directly observed karst conduits are just a small part of the whole karst system, and the complexity of the karst system is strongly uncertain; this uncertainty includes the location, density and connectivity of the conduit network (Pardo-Igúzquiza et al. 2011). Some researchers have demonstrated significant disturbance of conduit bifurcations using tracer tests (Goldscheider et al. 2008; Li 2012). Even in the synthetic case, the complexity of the network amplifies the variability in seawater intrusion compared with the single conduit (Sebben et al. 2015). Thus, comparing a double-conduit and single-conduit system is necessary for investigating seawater intrusion distance and influence on matrix salinity distribution. In addition, the geometry of the conduit is also a complex factor that needs to be considered in the flow calculation. Tam et al. (2004) pointed out that the sump in the conduit system acts as a barrier to delay the tracer transport process and results in a two-peak breakthrough curve. Field and Pinsky (2000) indicated that conduit irregularities may produce vortices and eddies in the groundwater flow and form an immobile fluid region. Hauns et al. (2001) used 3D computational fluid dynamics (CFD) code to investigate solute retardation by longitudinal changes in the conduit geometry, and they indicated that the retardation tends to be transformed to symmetrical dispersion with distance. In this study, the conduit surface irregularity is represented by surface structures, and the equation of local head loss is applied to calculate flow fluid through these structures.

Seawater intrusion is a dynamic process of variable-density fluid flow, and several numerical models have been developed for modeling variable-density groundwater flow in a porous medium, including SUTRA (Voss 1984), MOCDENSE (Sanford and Konikow 1985) and HST3D (Kipp 1997). SEAWAT

(Guo and Langevin 2002; Langevin et al. 2003; 2007) is a very popular numerical model for simulating coupled variable-density groundwater flow and solute transport. Xu et al. (2018a) used the SEAWAT model to investigate seawater intrusion in a costal karst aquifer and highlight the impacts of the conduit network. However, SEAWAT is limited in that it is only applicable for laminar groundwater flow by solving Darcy's equation in a porous medium; it is not suitable for the non-laminar flow in a karst aquifer. Non-laminar flow simulation is more complex than the laminar flow in porous media by Darcy's Law. Shoemaker et al. (2008) developed the MODFLOW-CFP model by coupling the conduit flow process (CFP) with MODFLOW (Harbaugh et al. 2000; Harbaugh 2005), which is applicable only in porous media based on Darcy's law. MODFLOW-CFP computes the transition of laminar flow and turbulent flow by the Reynolds number, and solves the turbulent flow in conduits using the Darcy-Weisbach equation. In various studies, Reimann and colleagues (Reimann et al. 2011, 2013, 2014) enhanced CFP by adding conduit-associated drainable storage (CADS) and a time-dependent boundary condition to investigate mass and heat transport in a karst aquifer. Xu et al. (2015a, 2015b) applied CFPv2 and UMT3D (Spiessl et al. 2007) to study nitrate transport and freshwater/seawater flow cycling in the Woodville Karst Plain of northern Florida (USA), a regional-scale well-developed karst aquifer. Thus, combining the variable-density flow equation and turbulent flow equation is essential for exploring seawater intrusion in coastal karst aquifers.

Xu and Hu (2017) developed the VDFST-CFP model to simulate density-dependent flow and salinity variation in a dual-permeability karst aquifer system. However, only two 2D synthetic horizontal and vertical benchmarks, with one conduit in each case, were discussed in the previous study. To enable the simulation of a more complicated conduit system and more accurate conduit flow calculation, this paper develops a double-conduit system based on the framework and algorithm in Xu and Hu (2017), fully discusses the vertical benchmark case, and investigates the influence of macro-structures and variations of conduit roughness on density flow simulation in a karst aquifer. These improvements provide insights on simulating more complex karst hydrology systems and on mitigating model uncertainty in a field application.

Mathematical methods

VDFST-CFP is a variable-density discrete-continuum numerical model for simulating density-dependent groundwater flow in karst aquifers with a conduit system. The hydrology and salt transport equations are solved under implicit iterative procedures. The groundwater flow field equation is affected by water density, which is determined by the salinity from the previous time step, and salinity is then calculated by the flow field for density computation in the next step. This iterative process is repeated within each time step until a convergence value of fluid density difference is reached. The density-dependent Darcy-Weisbach equation is applied on the groundwater flow in

the karst conduit, and is solved iteratively by the Newton-Raphson method (Xu and Hu 2017).

VDFST-CFP

In the dual-permeability model, the movement of density-dependent water in the porous media and conduit system is quantified by different equations. The finite-difference equations of SEAWAT (Guo and Langevin 2002; Xu and Hu 2017) are adopted in this study to describe variable-density flow and solute transport in porous media. Variable-density flow in a karst conduit is described by the density-dependent Darcy-Weisbach equation, which is derived from the Bernoulli and Darcy-Weisbach equations (Xu and Hu 2017):

$$Q = A\sqrt{\frac{2dg}{f}\left(\frac{\rho_f}{\rho}\frac{dh_f}{dl} - \frac{\rho - \rho_f}{\rho}\frac{dz}{dl}\right)} \qquad (1)$$

where Q is the volumetric flow rate [$L^3\ T^{-1}$]; A is the cross-sectional area perpendicular to the flow [L^2]; f is the friction factor [dimensionless]; d is the diameter of the karst conduit [L], g is the gravitational acceleration constant [LT^{-2}]; z is the elevation [L]; h_f is the equivalent freshwater head [L]; l is the karst pipe length [L].

The conduit system in Eq. (1) is discretized into several nodes and tubes (Fig. 1). The equivalent freshwater head and solute exchange with the porous medium are calculated at each node for every time step. The flow rate at a specific conduit node is

$$Q_n = Q_{n+1/2} + Q_{n-1/2} \qquad (2)$$

where Q_n is the volumetric flow rate at conduit node n [$L^3\ T^{-1}$]; $Q_{n\pm1/2}$ are the flow rates in the conduit pipes which are connected with nodes n and $n \pm 1$ [$L^3\ T^{-1}$].

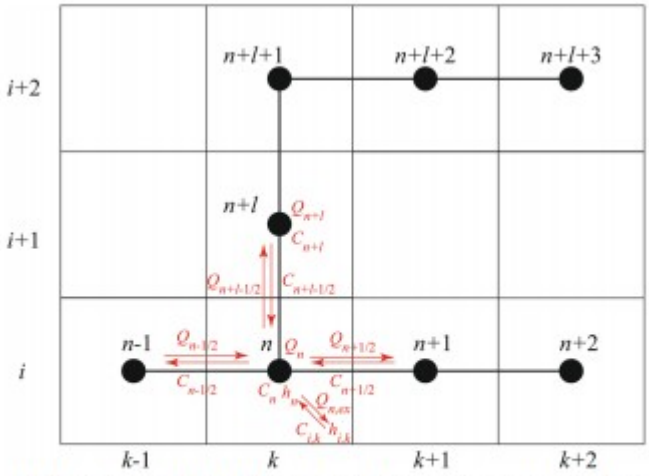

Fig. 1 Geometry and flow direction of the convergence point, including fluid flow in and flow out from surrounding tubes and exchanges with porous medium

This study considers complex conduits with several junctions. The multi-conduit network is more complex than the single-conduit system when considering the flow directions at the junction points. The nodal flow rate of the junction point is derived from Eq. (2) (Fig. 1),

$$Q_n = Q_{n+1/2} + Q_{n-1/2} + Q_{n+l-1/2} \tag{3}$$

where $Q_{n+l-1/2}$is the volumetric flow rate between conduit nodes n and $n + l$ [$L^3\ T^{-1}$].

The conduit transport can be described by the one-dimensional advection-dispersion equation as

$$\frac{\partial C_l}{\partial t} = -q_l \frac{\partial C_l}{\partial u} + D_{\text{dis}} \frac{\partial^2 C_l}{\partial u^2} \tag{4}$$

where C_l is the solute concentration [ML^{-3}] in the conduit tube l; q_l is the flow velocity in conduit tube l, which is calculated by the flow rate within conduits [LT^{-1}]; D_{dis} is the dispersion coefficient within the conduit.

The concentration at a specific conduit node is calculated by the following equation

$$C_n = \frac{\sum Q^+_{n,l} C_{n,l} + Q^+_{n,\text{ex}} C_{i,k} + \sum_s Q^+_{n,s} C_{n,s}}{Q^+_{n-1/2} + Q^+_{n+1/2} + Q^+_{n,\text{ex}} + \sum_s Q^+_{n,s}} \tag{5}$$

where C_n is the weighted arithmetic mean of the solute concentration [ML^{-3}] at conduit node n, which is determined by the flow rates and concentrations in neighboring conduit tubes, the exchanges with the surrounding porous medium, and sink/source terms (the superscript "+" indicates the inflow terms at conduit node n, and in this equation, only inflow terms are

considered in the concentration calculation); $C_{n,s}$ is the solute concentration of the sources or sinks in conduit node n [ML^{-3}]; $Q_{n,s}$ is the volumetric flow rate from the sources at conduit node n [$L^3\ T^{-1}$].; $C_{n,l}$ is the solute concentration in the neighboring tube l of node n [ML^{-3}]; $Q_{+n,l}Q_{n,l+}$ is the discharge from tube l into conduit node n [$L^3\ T^{-1}$]; $Q_{n,ex}$ is the exchange flow rate between node n and matrix block i,k [$L^3\ T^{-1}$]; $C_{i,k}$ is the solute concentration of matrix block i,k [ML^{-3}].

Conduit roughness

The density-dependent Darcy-Weisbach equation is used in this study for modeling laminar and turbulent flow in karst conduits. The Reynolds number is a key parameter in the transition between laminar and turbulent flow,

$$\mathrm{Re} = \frac{qD}{u} \qquad (6)$$

where Re is the Reynolds number [dimensionless]; q is the velocity based on the cross-sectional area of the conduit or pipe [LT^{-1}]; D is the conduit diameter [L]; u is the kinematic viscosity of the fluid [$L^2\ T^{-1}$].

Surface roughness determines the friction factor in the conduit flow calculation. The friction factor f [dimensionless] is determined by $f = \mathrm{Re}/64$ for laminar flow ($\mathrm{Re} < 4000$) (Reimann et al. 2011). For turbulent flow ($\mathrm{Re} >= 4000$), the relationship between the friction factor, the Reynolds number and the relative roughness is more complex; one model for this relationship is the Colebrook-White formula (Colebrook and White 1937; Shoemaker et al. 2008). However, the Colebrook-White formula is solved iteratively and is time-consuming; therefore, many historical approximations of the Colebrook-White equation have been developed (Zigrang and Sylvester 1982; Barr 1981; Romeo et al. 2002). The Goudar-Sonnad equation (Goudar and Sonnad 2008) is one of the approximation methods of the Darcy-Weisbach friction factor that is used in this paper. The applicable range of the Reynolds Number (Re) is 4000 to 10^8 for the Goudar-Sonnad equation,

$$\frac{1}{\sqrt{f}} = A[\ln(C/Q) + D_{\mathrm{CFA}}] \qquad (7)$$

where

$$A = \frac{2}{\ln(10)};\quad B = \frac{k_c}{3.71D};\quad C = \frac{\ln(10)\mathrm{Re}}{5.02}$$

$$Q = S^{s/(s+1)} \text{ where } S = B \cdot C + \ln(C)$$

$$D_{\mathrm{CFA}} = D_{\mathrm{LA}}\left(1 + \frac{Z/2}{(G+1)^2 + (Z/3)(2G-1)}\right)$$

where $G = B \cdot C + \ln\frac{C}{Q}$, $Z = \ln\frac{Q}{G}$, and $D_{\mathrm{LA}} = Z\frac{G}{G+1}$

The mean roughness height k_c is a key parameter for determining the friction factor in the conduit, which can be used as the average height of the micro-textures on the conduit wall,

$$k_c = \frac{1}{L}\int_0^L z(x)dx \quad (8)$$

where L is the length of the pipe [L]; x is the location of a certain structure or texture in the pipe [L], herein as the pipe wall surface; z is the height of the structure or texture corresponding to x [L].

Marco-structures of conduits

Surface roughness is conceptualized by the high-frequency, short-wavelength micro-structures on the surface of the pipe wall. However, macro-structure components in well-developed karst regions, including cavities on the conduit wall or stone stacking on the conduit bottom (Fig. 2a) that may strongly affect the friction factor and conduit flow, are addressed in this study. These macro-structures are considered as pipe expansions and contractions instead of diameter variations under high-resolution grid discretization (Fig. 2b and c). The conduit–matrix water exchange is calculated at each node of the conduit system, and is assumed to be unchanged with the variation in diameter within each tube. Expansion and contraction slow the conduit flow by producing additional head losses, which are referred to as local loss and are related only to the height, length, number of structures and the velocity of water flow into the structure. The friction head loss is defined as the regular head loss in the pipes due to the conduit wall friction factor. The local head loss is associated with the expansion and contraction, expressed in terms of loss coefficient (Cengel and Cimbaia 2004).

$$h_{\text{local}} = M\frac{V^2}{2g} \quad (9)$$

$$h_{\text{total}} = h_{\text{fric}} + h_{\text{local}} = \sum_i f\frac{L}{D}\frac{V_i^2}{2g} + \sum_j M_j\frac{V_j^2}{2g} \quad (10)$$

where h_{total} is the total head loss [L], h_{fric} is the friction head loss [L], and h_{local} is the local head loss [L]; i represents each pipe section with constant diameter, and j represents the number of a component that causes a local loss; M and M_j are loss coefficients [dimensionless]; L is the pipe length [L]; D is the constant diameter [L]; V_i is the flow velocity in a constant-diameter section [LT^{-1}]; V_j is the flow velocity of fluid that flows into the component j [LT^{-1}].

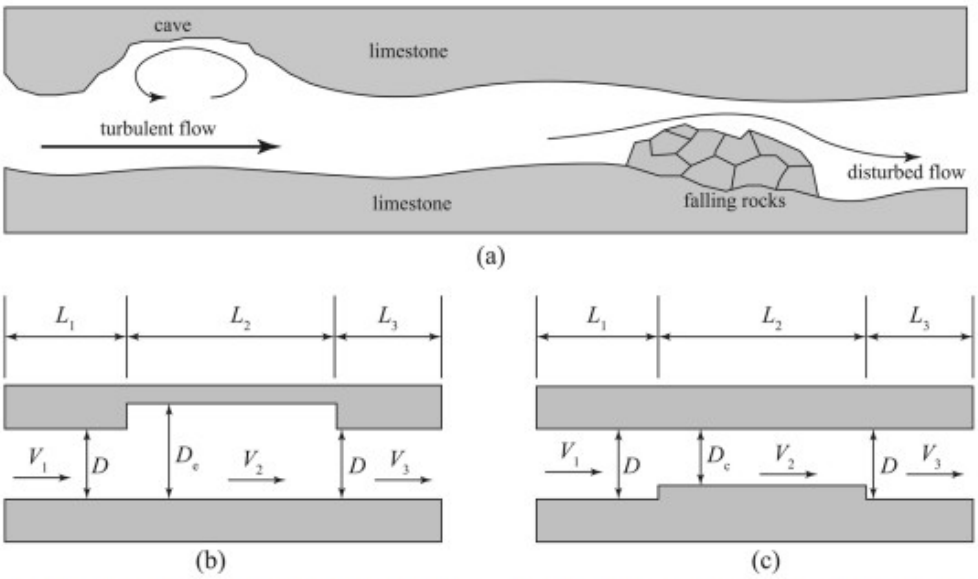

Fig. 2 **a** The cavity and rock stacking in the extensive karst conduit, which can be replaced by expansion and contraction in the model (represented in **b** and **c**, respectively). L_1 is the length before the structural component [L], L_2 is the length of the component [L], L_3 is the length after the component [L]; D is the diameter of the conduit [L]; D_e is the diameter of the expansion part [L]; D_c is the diameter of the contraction part [L]; V_1 is the flow velocity before the component [LT^{-1}], V_2 is the flow velocity at the component [LT^{-1}], and V_3 is the flow velocity after the component [LT^{-1}]

Assuming these macro-structures can be regarded as sudden contraction and expansion for simplification, the loss coefficients (M in Eq. (9)) are calculated using Eqs. (11) and (12) (Crane 2009). The gradual contraction and expansion could also be applied in these equations if divergence angles are determined; the relative equations are in reference to Crane Co. (Crane 2009).

$$M_{exp} = \frac{\left(1-\beta_e^2\right)^2}{\beta_e^4} \tag{11}$$

$$M_{con} = \frac{0.5\left(1-\beta_c^2\right)}{\beta_c^4} \tag{12}$$

where M_{exp} is the loss coefficient of expansion [dimensionless] and M_{con} is the loss coefficient of contraction [dimensionless]; β_e and β_c are the ratio of smaller diameter to larger diameter [dimensionless], for the expansion case, $\beta_e = D/D_e$, and for the contraction case, $\beta_c = D_c/D$.

Based on Eqs. (11) and (12), the total head loss of the conduit with an expansion that represents a cavity on the conduit wall, or a contraction which represents stones stacked on the bottom of the conduit, is expressed below, assuming that the exchange flows between the conduit and porous medium are constant among the neighbor expansion and contraction tubes.

$$V_1\pi\left(\frac{D}{2}\right)^2 = V_2\pi\left(\frac{D'}{2}\right)^2 = V_3\pi\left(\frac{D}{2}\right)^2 \tag{13}$$

$$h_{total} = \sum_i f\frac{L}{D}\frac{V_i^2}{2g} + \sum_j M_j\frac{V_j^2}{2g} \quad = f\frac{L_1+L_3}{D}\frac{V_1^2}{2g} + f\frac{L_2}{D'}\frac{V_2^2}{2g} + M_1\frac{V_1^2}{2g} + M_2\frac{V_2^2}{2g} \tag{14}$$

where in the expansion condition (Fig. 2b), $D' = D_e$, $M_1 = M_{exp}$, $M_2 = M_{con}$; in the contraction condition (Fig. 2c), $D' = D_c$, $M_1 = M_{con}$, $M_2 = M_{exp}$.

Local head loss can be expressed in terms of equivalent length L_{eq} (Cengel and Cimbaia 2004), for the conduit with an expansion (Fig. 2b):

$$\begin{aligned} &f\frac{L_2}{D_e}\frac{V_2^2}{2g} + \frac{\left(1-\beta_e^2\right)^2}{\beta_e^4}\frac{V_1^2}{2g} + \frac{0.5\left(1-\beta_e^2\right)}{\beta_e^4}\frac{V_2^2}{2g} = f\frac{L_{eq}}{D}\frac{V_1^2}{2g} \\ &\Rightarrow L_{eq} = L_2\beta_e^5 + \frac{D\left(1-\beta_e^2\right)^2}{f\beta_e^4} + \frac{D\left(1-\beta_e^2\right)}{2f} \end{aligned} \tag{15}$$

For the conduit with a contraction (Fig. 2c):

$$\begin{aligned} &f\frac{L_2}{D_c}\frac{V_2^2}{2g} + \frac{0.5\left(1-\beta_c^2\right)}{\beta_c^4}\frac{V_1^2}{2g} + \frac{\left(1-\beta_c^2\right)^2}{\beta_c^4}\frac{V_2^2}{2g} = f\frac{L_{eq}}{D}\frac{V_1^2}{2g} \\ &\Rightarrow L_{eq} = \frac{L_2}{\beta_c^3} + \frac{D\left(1-\beta_c^2\right)}{2f\beta_c^4} + \frac{D\left(1-\beta_c^2\right)^2}{f\beta_c^8} \end{aligned} \tag{16}$$

The total loss equation of expansion and contraction by using equivalent length is

$$h_{total} = f\frac{L_1 + L_3 + L_{eq}}{D}\frac{V_1^2}{2g} \tag{17}$$

Numerical simulation

Conceptual model

Figure 3 shows the conceptual model of seawater intrusion and brackish–freshwater exchange at a typical coastal karst aquifer. Seawater intrudes landward in two ways: (1) seawater gradually migrates through the porous medium and leads to a freshwater–seawater mixing zone in the coastal aquifer, and (2) seawater flows into submarine karst conduits when the hydraulic gradient is landward and contaminates freshwater further inland.

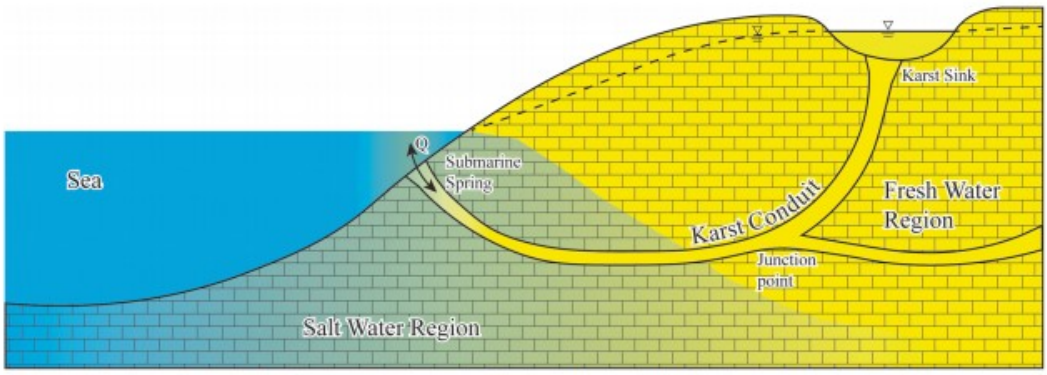

Fig. 3 Schematic cross section of a coastal karst aquifer. The submarine groundwater is directly connected with the inland karst spring by the karst conduit system with a junction point

Two synthetic benchmark models were set up to validate the VDFST-CFP model (Xu and Hu 2017): the horizontal benchmark was developed to verify the groundwater flow and solute transport simulation based on the discrete-continuum approach; the vertical case was used to evaluate the salt transport and relevant density-dependent flow in the model. This study modifies the vertical case based on Xu and Hu (2017) and shortens the length of cross section for both single-pipe and double-pipe vertical models. Meanwhile, the variable-density continuum SEAWAT model is developed and compared with the cases using the VDFST-CFP.

Model domain

It is difficult to simulate the karst process exactly at the field scale using the current version of VDFST-CFP without further optimization, due to the unaffordable computational cost for fine resolution of the discretization grid. A smaller 2D vertical benchmark than that of Xu and Hu's (2017) model is shown in Fig. 4. The spatial discretization of this aquifer system consists of 70 columns, 20 layers and one row. The widths of the row and column for each cell are both 15.24 m, and the thickness is 3.05 m in each layer. The elevation of the surface layer starts from 10.36 m below sea level (BSL) at the leftmost and gradually rises to 5.79 m BSL at the rightmost end. In the single-conduit model, the conduit system begins at the top of column 11, downward to layer 15, and then extends horizontally to column 68, and finally upward to the top of column 68 (Fig. 4a). In the double-conduit model, another conduit is added to the single-conduit model, which starts from layer 12, column 11, and then extends horizontally to connect with the vertical conduit at column 68 (Fig. 4b). In both models, the first and last nodes of the conduit system are set as submarine spring and inland karst spring, respectively.

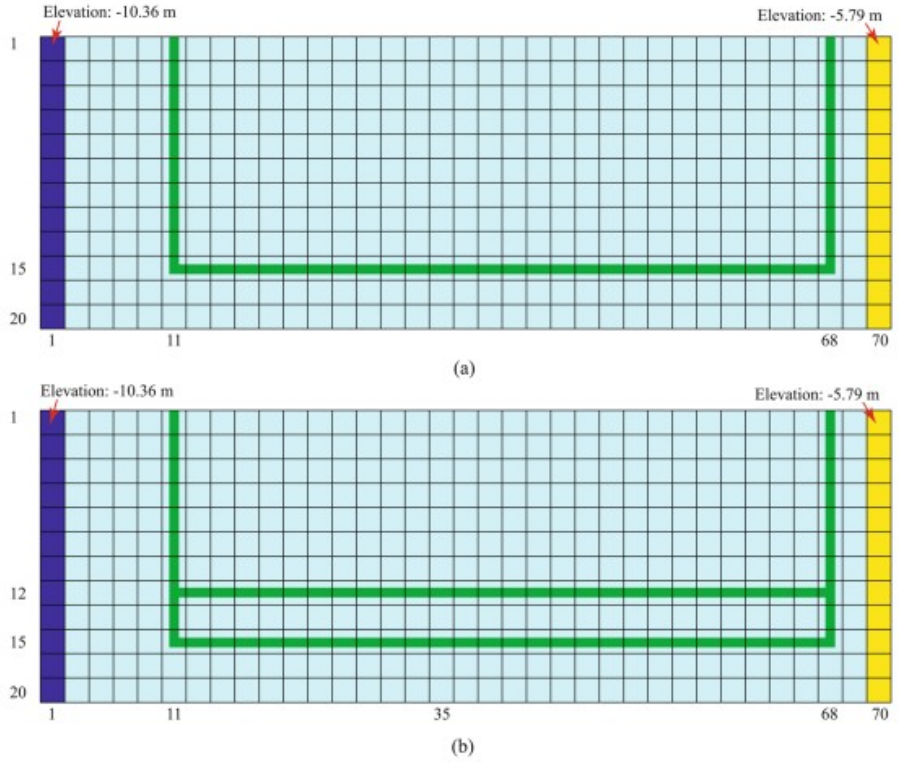

Fig. 4 Schematic finite-difference grid discretization and boundary conditions applied in the vertical benchmark case: **a** single-conduit model, **b** dual-conduit model. *Light blue cells* represent the porous medium; *green cells* represent the conduit system; *dark blue cells* represent the seawater boundary, for which the constant head is 0.0 m and constant concentration is 35.0 PSU; *yellow cells* represent the freshwater boundary, where the constant head is 1.07 m and constant concentration is 0.0 PSU

Boundary conditions and initial conditions

The aquifer is assumed to be confined, with no flow boundary on the bottom of this model. The freshwater boundary on the rightmost column is a constant head boundary of 1.07 m, and there is constant salinity of 0 practical salinity units (PSU); the seawater boundary on the leftmost column is set as 0.0 m constant head and 35.0 PSU constant concentration (Fig. 4). The values used for initial and boundary conditions are modified from previous studies (Xu and Hu 2017; Xu et al. 2018a; Davis et al. 2010). The conduit parameters determined based on the literature and field observations, along with the matrix parameters, are from field data.

The initial condition of hydraulic head in the porous medium gradually rises from 0.0 m at the leftmost column to 1.07 m at the rightmost column. The salinity in the porous medium is set to be 0.0 PSU at the beginning, except at the boundary condition. The initial conditions of conduit nodes and tubes are the same as those of the surrounding matrix cells, while the salinity and hydraulic head at the submarine spring (conduit node at column 11, layer 1) is 35.0 PSU and 0.0 m, respectively. Using the VDFST-CFP method, a rigorous convergence criterion for both the porous medium and conduits is needed, therefore, the time step size is specified as 0.0005 day.

Parameters

The parameter values of the porous medium aquifer used in this study are the same as those of Davis et al. (2010), who calibrated the parameter values in a regional hydraulic model in the Woodville Karst Plain of northern

Florida, based on observations, field data and a previous numerical study (Katz et al. 2004). For the high-resolution requirement of vertical discretization in variable-density numerical modeling, the parameters are listed in Table 1. However, similar to the conduit parameterization in Xu and Hu (2017), conduit diameter and mean roughness heights are synthetic instead of field-scale values, because of the limited applicability of the VDFST-CFP model for simulating large-diameter conduit networks. The parameters in the SEAWAT model are equivalent as the weighted arithmetic means from the parameters of the conduit and porous media in the VDFST-CFP model. The weights are calculated as the volume ratios of the matrix and conduit. The porosity and specific storage is assumed to be 1 in the conduit, and the dispersivity is set to 0, since advection is dominant process and dispersion is not considered in the conduit layer. In the VDFST-CFP model, the relationship between the hydraulic conductivity of the conduit in the SEAWAT model and the conduit diameter in the VDFST-CFP model is shown in Eq. (18) (Xu et al., 2017):

$$K = \frac{gD^2}{32v} \tag{18}$$

where K is the hydraulic conductivity of the conduit in the SEAWAT model [L^3 T^{-1}]; g is the gravitational acceleration [LT^{-2}]; D is the conduit diameter in the VDFST-CFP model [L]; v is the kinematic viscosity [L^2 T^{-1}].

Table 1 Parameters of the conduit system and porous media using the SEAWAT and VDFST-CFP models (Davis et al. 2010; Xu and Hu 2017; Xu et al. 2018a)

Parameter	Porous media	Conduit system, VDFST-CFP model	Conduit system, SEAWAT model
Hydraulic conductivity (m/day)	2286.0	–	1.5e6
Porosity	0.003	–	0.005
Specific storage	5e-5	–	0.001
Dispersivity (m)	10.0	–	0
Diameter (m)	–	0.24	–
Mean roughness height (m)	–	0.0024	–

Simulation results

Results of single-pipe and double-pipe models

Figure 5 shows the seawater intrusion results simulated by the VDFST-CFP model and the comparable SEAWAT model results in single-pipe and double-pipe scenarios after 0.2 days. High-density seawater flows into the system from the leftmost constant-head boundary and submarine spring, and the

seawater front moves further landward in the conduit system than in the surrounding matrix. The salinity distribution in the conduit system is further extended, and intrudes into the surrounding matrix via exchange through the pipe wall , thus contaminating the freshwater in the matrix. This exchange is not accurately simulated in the SEAWAT model, because the flow and solute transport through the conduit layer are extremely fast under Darcy's Law. The seawater–freshwater mixing zone in the matrix strongly follows the solute transport in the conduit layer, and the contamination plume in the porous medium in the double-pipe scenario is also larger and longer than that in the single-pipe system in the SEAWAT model. The simulated seawater front in the VDFST-CFP model is further landward than that in the SEAWAT model, due to the limitation of laminar flow computed by the Darcy equation in the SEAWAT model. The Reynolds number in the conduit system of the VDFST-CFP model is from 3000 to 1.2e+5, which represents turbulent flow. Darcy's equation defines a linear relationship between the hydraulic gradient and specific discharge, and non-laminar groundwater flow within the conduit system is overestimated. In the double-pipe model of the VDFST-CFP model, seawater intrusion obviously extends further landward in the deep conduit than the shallow one, since the hydraulic gradient is larger with higher equivalent freshwater head in the deeper conduit network. This updated version of VDFST-CFP provides the possibility for further studies on more complex conduit systems in a coastal karst aquifer.

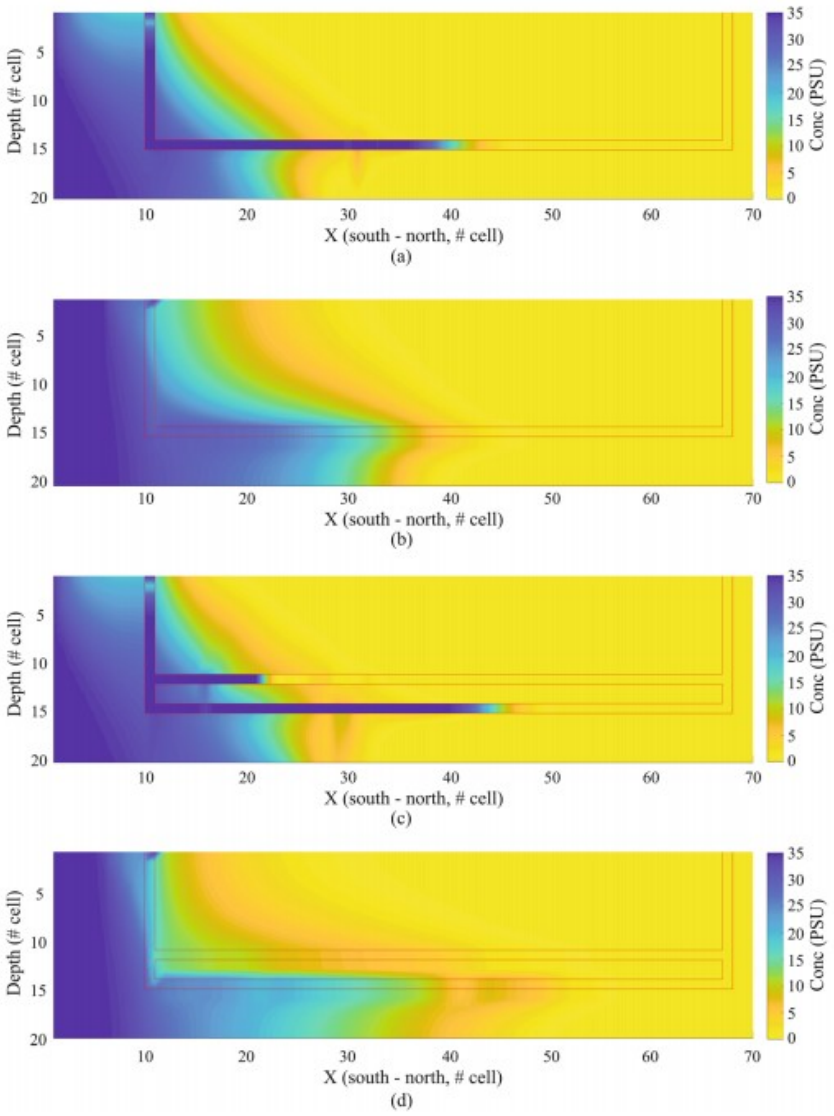

Fig. 5 Salinity simulations of the vertical benchmark. **a** seawater intrusion in a single-pipe model of the VDFST-CFP model; **b** seawater intrusion in a single-pipe model of the SEAWAT model; **c** seawater intrusion in a double-pipe model of the VDFST-CFP model; **d** seawater intrusion in a dual-pipe model of the SEAWAT model. *Blue* represents high concentration, *yellow* represents low concentration

Parameter sensitivity analysis

The parameter sensitivities are evaluated in order to assess the control factors in simulating seawater intrusion distance in both conduit and porous media using the updated version of the VDFST-CFP model. The evaluated factors are porous medium parameters including hydraulic conductivity (2286–2971 m/day), dispersivity (10–13 m), exchange interaction (2286–2971 m/day), porosity (0.003–0.0039) and specific storage (5.0e-5–6.5e-5), and conduit parameters including diameter (24.4–31.7 cm) and friction factor (0.0379–0.0492). The composite scale sensitivity (CSS) values are calculated by forward approximation on these seven parameters (Hill and Tiedeman 2006):

$$\mathrm{CSS}_j = \sum_{i=1}^{N} \left(\frac{\mathrm{DSS}_{ij}{}^2}{N} \right)^{1/2} \tag{19}$$

$$\mathrm{DSS}_{ij} = \frac{y_i'(b + \Delta b) - y_i'(b)}{\Delta b_j} |b_j| w_i^{1/2} \tag{20}$$

where CSS_j is the composite scaled sensitivity of the jth parameter; N is the number of observations; DSS_{ij} is the dimensionless scaled sensitivity of the ith observation with respect to the jth parameter; y′iyi′ is the result of the ith observation; $b_j$is the jth estimated parameter; b is the parameter vector; Δb is a vector of zero, except that the jth parameter equals Δb_j, and Δb_j should be no more than 5% of b_j(Saltelli et al. 2000); w_i is the weight of the ith observation, which is calculated in this paper by the inverse of the standard deviation; the standard deviation is 0.003 m for head measurement and 0.1 PSU for salinity measurement, according to some field studies in Florida (Shoemaker 2004; Xu et al. 2018a). A larger CSS value indicates that the certain parameter is more important to the simulation results. The results of the parameter effects on the single-pipe and double-pipe modeling simulations are shown in Fig. 6. In parameter sensitivity analysis, the conduit simulations are evaluated at all conduit nodes, and the matrix simulations are evaluated throughout layer 7, which is 15.24 m above the conduit system.

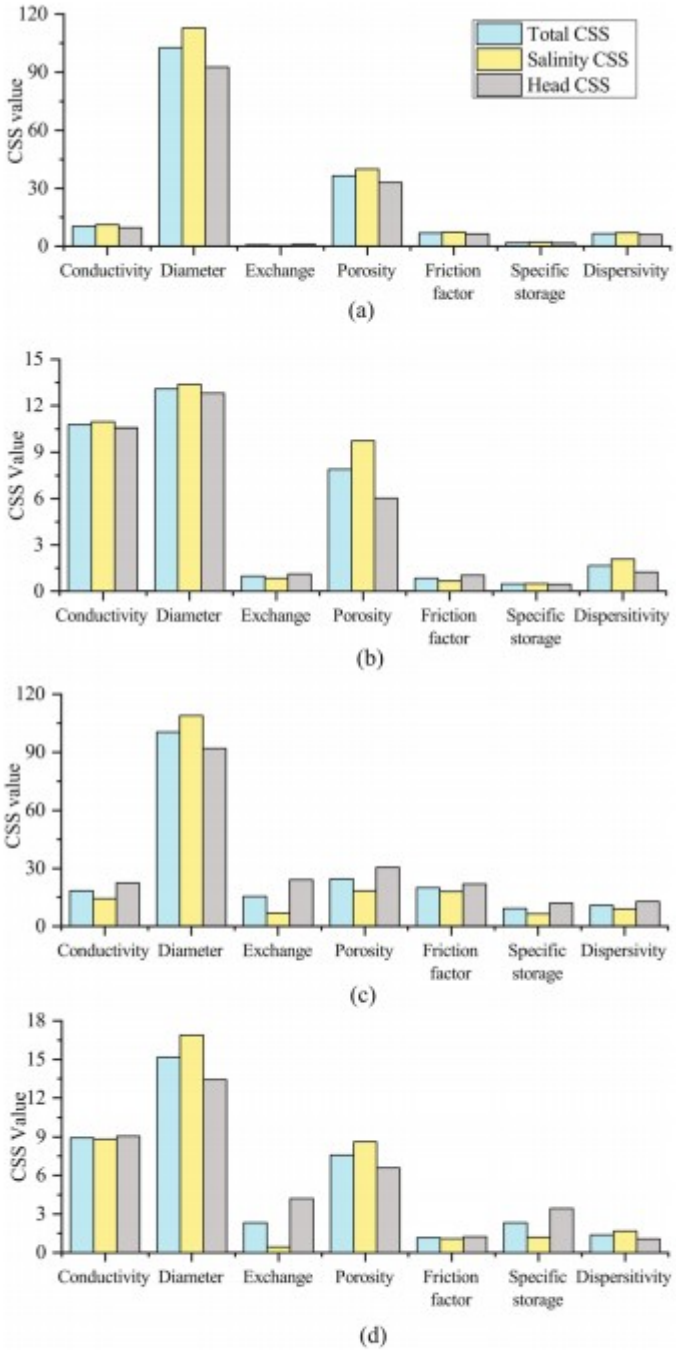

Fig. 6 The composite scale sensitivity (CSS) values of the single-pipe and double-pipe systems: **a** conduit simulation in a single-pipe system; **b** matrix simulation in a single-pipe system; **c** conduit simulation in a double-pipe system; **d** matrix simulation in a double-pipe system

The similar CSS values of the single-pipe and double-pipe systems indicate that the parameter sensitivity results are consistent across various scenarios. The influence of diameter in the conduit and matrix simulations is seen mainly with the largest CSS values, because the diameter significantly

determines the flow rate computed by the Darcy-Weisbach equation. The hydraulic head and salt distribution in the conduit are highly affected by the change in conduit flow velocity, which then influences the salinity distribution in the porous media through the conduit–matrix exchange. Like the conduit diameter, the friction factor also influences the flow rate in the Darcy-Weisbach equation; the significance of the friction factor is small to the matrix simulation but relatively large to the conduit simulation, especially in the double-conduit scenario. As a result, the investigation of the macro-structure, which changes the conduit diameter and friction factor, is very important and will be discussed in the next section. Hydraulic conductivity is a major parameter in the Darcy equation and plays a significant role in the matrix simulation. This is different from the conclusion of Xu and Hu (2017) because of the different location evaluated for the matrix simulation. The matrix simulations are evaluated 15.24 m above the major conduit network in this study, while Xu and Hu (2017) measured the matrix simulation exactly where the conduit nodes of the porous medium cells were located. Porosity is another important parameter. The solutions of the flow field and transport equation are coupled with each other, and the hydraulic head is determined by the salinity distribution in each time step. In addition, porosity significantly affects the conduit flow via exchange due to the fast seepage velocity near the conduit. Therefore, the value of porosity strongly influences both the head and salinity calculations in the porous medium and conduit systems. In this study, porosity is surprisingly more important than hydraulic conductivity in conduit simulation. This underestimation of hydraulic conductivity sensitivity is counterintuitive, and highlights the uncertainty of hydraulic conductivity in simulating non-Darcian flow in a porous medium near a conduit system. The exchange rate variation is not significant to the results in the conduit and matrix, which is consistent with Xu and Hu (2017), probably because of the small head difference between the conduit and matrix. Dispersion is not an important parameter, because salinity transport in the system is dominated by high-velocity advection, with negligible dispersion. Matrix simulations show higher sensitivity to the matrix parameters such as hydraulic conductivity and effect porosity than conduit simulation. Compared to the single-pipe system, the matrix-conduit exchange, friction factor and specific storage are more important to the matrix simulation in the double-pipe system, while the significance of hydraulic conductivity and porosity decreases in the double-pipe system. The difference between the two scenarios can possibly be explained by the greater water flow into the conduit system in the double-pipe system; in this case, the parameters of the conduit, especially conduit diameter, play a more important role in seawater intrusion simulation.

Effect of macro-structures

The macro-structures on the conduit wall are considered as expansions and contractions by the variation in conduit diameter (section *Macro-structures of conduits*), which is also an indicator of the karst conduit roughness

complexity. Here, the inter-comparison of macro-structures and mean roughness height (section *Macro-structures of conduits*) with regard to seawater intrusion distance in the single-pipe system is studied. Five cases with different macro-structures are listed in Table 2 (group 1); the length of expansion and contraction are both set (L_2 in Fig. 2) as 0.76 m, and the diameter difference ($D_e - D$ for expansion and $D - D_c$ for contraction in Fig. 2) is 0.06 m. The original conduit diameter is set as 0.24 m, the same as that in Table 1. The equivalent mean roughness height of these macro-structures in each case is calculated by Eq. (8) and listed in Table 2 (group 2); case 1 is the standard case which is calculated in section *Results of single-pipe model and double-pipe model*.

Table 2 The macro-structures for each case; their equivalent mean roughness height is calculated by Eq. (8). The friction factor is calculated from mean roughness and the Reynolds number, while the Reynolds number (ranging from 3000 to 1.2e5) is calculated in a dynamic process, since flow velocity is changing in the simulation process. Thus, the friction factor in this table is just a reference, and not the real values in the numerical simulation

Case	Macro-structures (group 1)	Equivalent mean roughness height (m) (group 2)	Equivalent friction factor (group 2)
Case 1 (standard case)	none	0.0024	0.0379
Case 2	1 expansion and 1 contraction	0.0082	0.0600
Case 3	2 expansion and 2 contraction	0.0140	0.0763
Case 4	3 expansion and 3 contraction	0.0201	0.0915
Case 5	4 expansion and 4 contraction	0.0259	0.1050

The five cases of seawater intrusion distance under variation of macro-structure are shown in Fig. 7. The number of macro-structures and mean roughness height both play important roles with regard to seawater intrusion in the conduit system. Seawater intrudes less landward through the conduit network with more structural components and higher roughness height, while the variation in the number of components and the mean roughness height are not significant to seawater intrusion in the matrix. The effect of macro-structures (group 1) produces about 1–2 cells (nearly 5%) less landward seawater intrusion in terms of distance in the conduit than the cases with equivalent roughness (group 2). Although the results of using macro-structures and equivalent mean roughness height are very close in this study, the expansion and contraction method avoids the limitation of a small applicable range for mean roughness height when the friction factor becomes unacceptably large.

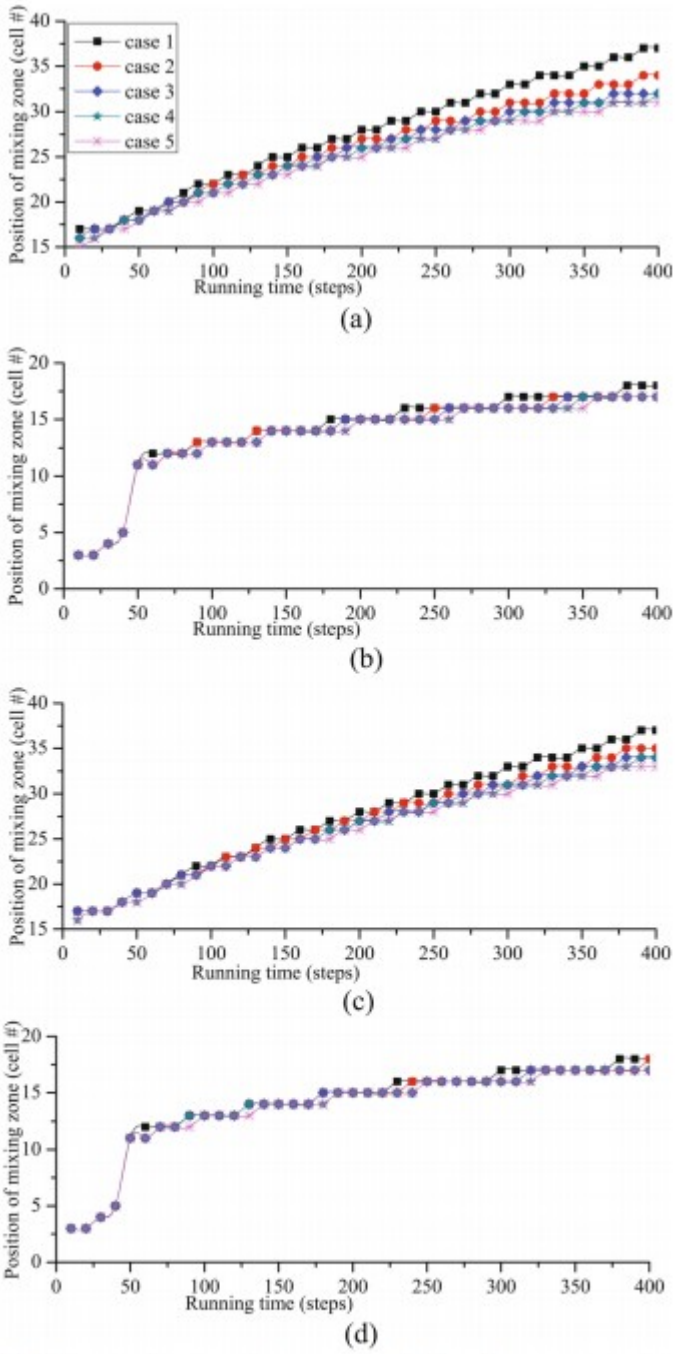

Fig. 7 Seawater intrusion distance under variation of macro-structure in **a** conduit simulation and **b** matrix simulation, and seawater intrusion distance under variation of equivalent mean roughness height in **c** conduit simulation and **d** matrix simulation. Cases 1–5 are with respect to parameters listed in Table 2

Conclusion and discussion

VDFST-CFP is a numerical model for simulating variable-density flow in a dual-permeability system, particularly for seawater intrusion in a coastal karst aquifer (Xu and Hu 2017). In this study, the original VDFST-CFP model

is improved with the capability of multi-conduit simulation and a better description of conduit wall roughness. The flow and transport equations at the junction point of the conduit system are modified. Currently, the multi-conduit system model simulates only two pipes, since the computational cost becomes significant when even a single pipe is added. The major computational cost in using the VDFST-CFP model involves solving the non-linear flow equation by Newton's iteration in the conduit system. A sensitivity analysis of parameters shows that hydraulic conductivity, conduit diameter and porosity are the three most important parameters, and diameter is the most important factor in controlling intrusion distance, since it strongly influences the flow rate in the conduit tubes. The diameter variation in the karst conduit by contraction and expansion will be discussed in the next paragraph. Conduit diameter becomes even more significant in the double-conduit system, since more water flows into the conduit. A larger contamination plume is found in the dual-conduit system when a shallow pipe is added in the system with more complex and extensive seawater–freshwater interaction in this double-conduit scenario. This result indicates that the actual seawater intrusion condition and environmental status are even worse than those determined using the former modeling estimation, when considering more complex systems in a real coastal aquifer.

This study also improves the conduit structure and geometry using expansion and contraction of micro- and macro-structures. The size of the micro-structures on the conduit wall is considered as mean roughness height in the density-dependent conduit flow, and implemented in the Goudar-Sonnad equation (Goudar and Sonnad, 2008). In this work, larger mean roughness height results in less landward seawater intrusion. The large structures on the conduit wall, on the other hand, are considered as contraction and expansion, which may cause additional local head loss due to energy loss at the small structures on the conduit wall. This study provides a modeling method to take both friction and local head loss into account in the flow of karst conduit systems, and reveals the significant effects of large conduit wall components on flow simulation. A parameter sensitivity study shows that more components lead to slower seawater intrusion in conduits, but they have little effect on salinity transport in the matrix. An inter-comparison test is set up with five different pairs of macro-structures and five equivalent large mean roughness heights. The results show that seawater intrusion cases are similar between the case of macro-structures and equivalent mean roughness height, although 5% more landward intrusion can be found with macro-structures. The method of using local head loss by macro-structures has a larger applicable range for friction factors, since the equivalent mean roughness height is larger than 1/10 of the diameter when considering four pairs of macro-components.

The current study aimed to investigate seawater intrusion in a synthetic coastal karst aquifer with the effect of multiple pipes and pipe structures; hence all the simulations are transient flow due to the salinity variation

calculation. This study does not evaluate groundwater pumping effects on karstic coastal aquifers, as most pumping wells are not located exactly at the conduit or right above the conduit. VDFST-CFP only simulates seawater intrusion through the conduit network in the surrounding matrix in the 2D cross section where the conduit network is located. However, the pumping effect will be important when VDFST-CFP is extended to simulate seawater intrusion in a 3D domain. Xu et al. (2018a) also analyzed the effect of sea level variation and rainfall period by the SEAWAT model. Also, related investigations regarding sea level and precipitation using the VDFST-CFP method may be conducted in the future. Other limitations of this model are grid resolution restriction and computation burden. The numerical accuracy of the VDFST-CFP model is controlled by the conduit diameter and Newton-Raphson method criteria (Xu and Hu 2017); the mass balance error becomes unacceptable when the model has even coarser spatial and temporal resolution. The acceptable range of mass balance error is 2%. This error is larger with the double-pipe than the single-pipe model in most cases due to more complex density calculation. These limitations are the largest obstacle to applying the VDFST-CFP model to a real-world case. Future studies should investigate how to improve simulation accuracy and reduce the computational burden; also, complex conduit systems and conduit wall structures can be further studied to expand the application of the VDFST-CFP model.

Acknowledgements

The authors would like to thank Dr. Ming Ye, Dr. Stephen Kish and Dr. Yang Wang at Florida State University for providing useful insights and comments during the development of the conceptual model and numerical modeling. This project is partially funded by the National Natural Science Foundation of China (grant number 41530316) and partially by Osmond Tanner Endowment.

References

Arfib B, Cavalera T, Gilli E (2006) Influence de l’hydrodynamique sur l’intrusion saline en aquifer karstique cotier (Influence of hydrodynamics on saline intrusion in the karstic coastal aquifer). Compt Rendus Geosci 338(11):757–767

Barr DIH (1981) Solutions of the Colebrook-White function for resistance to uniform turbulent flow. Proc Inst Civ Eng 71:529–535

Bear J, Cheng AHD, Sorek S, Ouazar D, Herrera I (1999) Seawater intrusion in coastal aquifers. Springer Science & Business Media

Cengel, Y, Cimbaia (2004) Fluid mechanics fundamentals and applications. McGraw-Hill Science/Engineering/Math,1024 pp

Colebrook CF, White CM (1937) The reduction of carrying capacity of pipes with age. J Inst Civ Eng 7:99–118

Crane Co (2009) Flow of fluids through valves, fittings and pipes. Crane Technical Paper no 410. Crane Co., Stamford, 132 pp

Davis JH, Verdi R (2014) Groundwater flow cycling between a submarine spring and an inland fresh water spring. Groundwater 52(5):705–716

Davis JH, Katz BG, Griffin DW (2010) Nitrate-N movement in groundwater from the land application of treated municipal wastewater and other sources in the Wakulla Springs Springshed, Leon and Wakulla counties, Florida, 1966-2018. US Geological Survey Scientific Investigations Report 2010-5099, 90 pp

Field MS, Pinsky PF (2000) A two-region nonequilibrium model for solute transport in solution conduits in karstic aquifers. J Contam Hydrol 44:329–351

Fleury, P., Bakalowicz, M. and de Marsily, G. (2007) Submarine springs and coastal karst aquifers: a review. J Hydrol 339(1):79–92

Goldscheider N, Meiman J, Pronk M, Smart C (2008) Tracer tests in karst hydrogeology and speleology. Int J Speleol 37(1)

Goudar CT, Sonnad JR (2008) Comparison of the iterative approximations of the Colebrook-White equation: Here's a review of other formulas and a mathematically exact formulation that is valid over the entire range of re values. Hydrocarb Process 87(8)

Guo W, Langevin C (2002) User's guide to SEAWAT: a computer program for simulation of three-dimensional variable-density ground-water flow. US Geological Survey Techniques of Water-Resources Investigations, Book 6, Chapter A7, 77 pp

Harbaugh AW (2005) MODFLOW-2005, the US Geological Survey modular ground-water model: the ground-water flow process. US Department of the Interior, US Geological Survey, Reston, VA, USA

Harbaugh AW, Banta ER, Hill MC, McDonald MG (2000) MODFLOW-2000, the US Geological Survey modular ground-water model: User guide to modularization concepts and the ground-water flow process. US Geological Survey, Reston, VA, USA

Hauns M, Jeannin PY, Atteia O (2001) Dispersion, retardation and scale effect in tracer breakthrough curves in karst conduits. J Hydrol 241:177–193

Hill MC, Tiedeman CR (2006) Effective groundwater model calibration: with analysis of data, sensitivities, predictions, and uncertainty. Wiley, 480 pp

Katz BG, Chelette AR, Pratt TR (2004) Use of chemical and isotopic tracers to assess nitrate contamination and ground-water age, Woodville Karst Plain, USA. J Hydrol 289(1):36–61

Kipp KL (1997) Guide to the revised heat and solute transport simulator: HST3D-Version 2. US Geological Survey Water-Resources Investigations Report 97-4157, 149 pp

Langevin CD, Shoemaker WB, Guo W (2003) MODFLOW-2000, the US Geological Survey Modular Ground-Water Model--Documentation of the SEAWAT-2000 Version with the Variable-Density Flow Process (VDF) and the Integrated MT3DMS Transport Process (IMT). US Department of the Interior, US Geological Survey, Open File Report, 43 pp

Langevin CD, Thorne DT, Dausman AM, Sukop MC, Guo W (2007) SEAWAT Version 4: A Computer Program for Simulation of Multi-Species Solute and Heat Transport. US Geological Survey Techniques and Methods Book 6, Chapter A22, 39 pp

Li G (2012) Calculation of karst conduit flow using dye tracing experiments. Transp Porous Med 95:551–562

Pardo-Igúzquiza E, Durán-Valsero JJ, Rodríguez-Galiano V (2011) Morphometric analysis of three-dimensional networks of karst conduits. Geomorphology 132:17–28

Reimann T, Geyer T, Shoemaker WB, Liedl R, Sauter M (2011) Effects of dynamically variable saturation and matrix-conduit coupling of flow in karst aquifers. Water Resour Res 47(11)

Reimann T, Liedl R, Giese M, Geyer T, Maréchal J-C, Dörfliger N, Bauer S, Birk S (2013) Addition and Enhancement of Flow and Transport processes to the MODFLOW-2005 Conduit Flow Process. 2013 NGWA Summit-The National and International Conference on Groundwater, 28 April–2 May San Antonio, TX

Reimann T, Giese M, Geyer T, Liedl R, Maréchal J-C, Shoemaker WB (2014) Representation of water abstraction from a karst conduit with numerical discrete-continuum models. Hydrol Earth Syst Sci 18(1):227–241

Romeo E, Royo C, Monzon A (2002) Improved explicit equations for estimation of the friction factor in rough and smooth pipes. Chem Eng J 86:369–374

Saltelli A, Chan K, Scott EM (2000) Sensitivity analysis. John Wiley & Sons, 465 pp

Sanford WE, Konikow LF (1985) A two-constituent solute-transport model for ground-water having variable density. US Geological Survey Water-Resources Investigations Report 85-4279, 88 pp

Sebben ML, Werner AD, Graf T (2015) Seawater intrusion in fractured coastal aquifers: a preliminary numerical investigation using a fractured Henry problem. Adv Water Resour 85:93–108

Shoemaker WB (2004) Important observations and parameters for a salt water intrusion model. Ground Water 42:829–840

Shoemaker WB, Kuniansky EL, Birk S, Bauer S, Swain ED (2008) Documentation of a conduit flow process (CFP) for MODFLOW-2005. US Geological Survey Techniques and Methods, Book 6, Chapter A24, 50 pp

Spiessl SM, Prommer H, Licha T, Sauter M, Zheng C (2007) A process-based reactive hybrid transport model for coupled discrete conduit–continuum systems. J Hydrol 347(1):23–34

Tam VT, Trung ND, Ke DT, Attrlaan O (2004) Interpretation of a cave system based on tracer experiment, geostructure and cave development analysis. Trans-KARST 2004, Proceedings of the International Transdisciplinary Conference on Development and Conservation of Karst Regions, 13–8 September 2004, Hanoi, Vietman

Voss CI (1984) A finite-element simulation model for saturated-unsaturated, fluid-density-dependent ground-water flow with energy transport or chemically-reactive single-species solute transport. US Geological Survey Water-Resources Investigation Report 84-4369, 409 pp

Werner AD et al (2013) Seawater intrusion processes, investigation and management: recent advances and future challenges. Adv Water Resour 51:3–26

Xu Z, Hu BX (2017) Development of a discrete-continuum VDFST-CFP numerical model for simulating seawater intrusion to a coastal karst aquifer with a conduit system. Water Resour Res 53:688–711. https://doi.org/10.1002/2016WR018758

Xu Z, Hu BX, Davis H, Cao J (2015a) Simulating long term nitrate-N contamination processes in the Woodville Karst Plain using CFPv2 with UMT3D. J Hydrol 524:72–88

Xu Z, Hu BX, Davis H, Kish S (2015b) Numerical study of groundwater flow cycling controlled by seawater/freshwater interaction in a coastal karst aquifer through conduit network using CFPv2. J Contam Hydrol 182:131–145

Xu Z, Bassett SW, Hu BX, Dyer SB (2016) Long distance seawater intrusion through a karst conduit network in the Woodville Karst Plain, Florida. Sci Rep 6:32235

Xu Z, Hu BX, Ye M (2018a) Numerical modeling and sensitivity analysis of seawater intrusion in a dual-permeability coastal karst aquifer with conduit networks. Hydrol Earth Syst Sci 22:1–19

Xu Z, Massei N, Padilla I, Hartmann A, Hu B (2018b) Characterization, modelling and remediation of karst in a changing environment. Environ Earth Sci 77(12):476

Zigrang DJ, Sylvester ND (1982) Explicit approximations to the solution of Colebrook’s friction factor equation. AIChE J 28:514–515